Accepted Manuscript

Carbon Nanotube Schottky type Photodetectors for UV applications

A. Filatzikioti, N. Glezos, V. Kantarelou, A. Kyriakis, G. Pilatos, G. Romanos, T. Speliotis, D.J. Stathopoulou

PII: S0038-1101(18)30365-4
DOI: https://doi.org/10.1016/j.sse.2018.10.018
Reference: SSE 7486

To appear in: *Solid-State Electronics*

Received Date: 23 June 2018
Revised Date: 27 September 2018
Accepted Date: 26 October 2018

Please cite this article as: Filatzikioti, A., Glezos, N., Kantarelou, V., Kyriakis, A., Pilatos, G., Romanos, G., Speliotis, T., Stathopoulou, D.J., Carbon Nanotube Schottky type Photodetectors for UV applications, *Solid-State Electronics* (2018), doi: https://doi.org/10.1016/j.sse.2018.10.018

This is a PDF file of an unedited manuscript that has been accepted for publication. As a service to our customers we are providing this early version of the manuscript. The manuscript will undergo copyediting, typesetting, and review of the resulting proof before it is published in its final form. Please note that during the production process errors may be discovered which could affect the content, and all legal disclaimers that apply to the journal pertain.

ACCEPTED MANUSCRIPT

Carbon Nanotube Schottky type Photodetectors for UV applications

A.Filatzikioti[a], N.Glezos[b], V. Kantarelou[c], A.Kyriakis[c] , G.Pilatos[b] , G.Romanos[b], T. Speliotis[b] and D.J.Stathopoulou[a]

[a]*National Technical University of Athens, Iroon Polytexneiou 9, 157 80 Athens, Greece*

[b]*Institute of Nanoscience and Nanotechnology, NCSR Demokritos, Aghia Paraskevi, Athens 15310, Greece*

[c]*Institute of Nuclear and Particle Physics, NCSR Demokritos, Aghia Paraskevi, Athens 15310, Greece*

Abstract

Multiple wall carbon nanotubes (MWCNT) present advantages for optoelectronic applications such as the large effective photo-collector surface as well as the possibility to tune their band gap and absorbance through the growth parameters. We demonstrate a hybrid MWCNT/Si_3N_4/n-Si photodetector based on ordered MWCNTs and evaluate its performance in the UV, visual and near IR spectrum (200-1000nm). The basic device and some meaningful variations including additional layers are electrically and optically tested and compared. The overall results suggest that all devices had a satisfactory performance in the visual part of the spectrum and that the basic structure had the better performance as a UV detector (EQE 90% @ 275nm@ 7V). The aim of this work is to demonstrate that the growth of dense ordered MWCNTs can be successfully combined with other semiconductor clean room processes in order to fabricate photodetectors, provided that the side effects are taken into account and the process flow is selected appropriately.

Keywords: carbon nanotube photodetector, Schottky barrier, MIS detector, UV detector, thermionic emission, Richardson method, Norde Method

ACCEPTED MANUSCRIPT

ACCEPTED MANUSCRIPT

1. Introduction

Carbon nanotubes (CNT) along with other carbon allotropes like fullerenes, quantum dots and graphene have attracted great interest because of their unique optoelectronic properties that may lead to novel photosensitive devices. The advantages of these materials are their tunable bandgap, high absorption coefficients and high charge carrier mobility [1],[2]. Several photodevices have appeared, based either on single wall (SWCNT)[3],[4], [5], multiple wall carbon nanotubes (MWCNT)[6],[7] or combinations with graphene[8] using diverse geometries such as planar metal-semiconductor-metal (MSM) or vertical metal-insulator-semiconductor (MIS) structures.

The use of CNTs in detector devices for infrared has attracted particular attention[4], [7], [9]. The combination of CNTs with conventional semiconductors and metals to form a device presents technological challenges because of the high temperatures required for the production of CNTs and the catalysts used (e.g. Fe). These conditions may result in structural modifications of the substrate specially when the CNT formation temperature approaches the formation temperatures of other layers or even cause metal migration. One way to circumvent these problems is the separate preparation of CNTs in solution[10], [11]. The drawback of using CNTs from solution is that the effective area of the sensor is limited and this effects the responsivity of the device. On the other hand the use of ordered free-standing MWCNTs for photodevices[12] presents advantages, since they have a tunable absorbance depending on their height while their ordering results in a large effective area sensor. Additionally the bandgap depends on their thickness, thus it is tunable by changing the formation conditions.

In this work we fabricated and evaluated a hybrid MWCNT/Si_3N_4/n-Si photodetector based on ordered dense MWCNTs. The intermediate silicon nitride layer is conductive because of the contamination from the Fe catalyst (Ferrocene, present in MWCNT growth process) and the Au electrode and its conductance is regulated by its thickness. The basic device shows adequate responsivity in the UV and visible part of the spectrum. Along with this device we also fabricated two variations, one with an additional Si_3N_4 layer on the backside (device NC) and one with an Indium Tin Oxide (ITO) film which overlaps the MWCNT film and the Au electrode (device CI). We investigated the effect of the inclusion of these layers in the basic device (C) by studying the electrical and optical properties.

2. Experimental

2.1 Device preparation

The devices were built on (100) n-Si substrates of 10Ω.cm resistivity. The first step was to deposit a 140nm Si_3N_4 film on the top side to serve as a diffusion barrier for the metals involved by a Tempress LPCVD system at 800 ^oC with source gases ammonia and dichlorosilane as source gases. This process -as is known- deposits the same layer on the

ACCEPTED MANUSCRIPT

back side of the wafer. On a part of the samples the back side Si_3N_4 film was removed in order to study this effect on device performance. A Cooke 401 DC magnetron sputtering was used for electrode deposition (5nm Cr followed by 30nm Au). The backside electrode covered the whole surface, while the front contacts shaped as disks of 3mm diameter were deposited through a shadow mask.

For the MWCNT array deposition a home-made CVD reactor was used (Fig. 1a). A mixture of 2g of Camphore ($C_{10}H_{16}O$, Sigma – Aldrich 21310, 95% purity) with 0.1g of Ferrocene (Sigma–Aldrich F408, 98% purity) used as a catalyst was injected into the device with the use of N_2 gas flow (0.6 l/min)[9]–[13]. After a preheating phase at T = 200 ^oC the mixture gas travels through the main high temperature oven operating at 850 ^oC. A steel mask was used to define growth areas in the form of 5mm diameter disks. A dense uniform layer of MWCNTs was produced this way on the substrates which were placed at the center of the furnace's hot zone. The MWCNTs produced were 20nm in diameter and 20μm in height (Fig 1b). The whole process lasted about 40min. The MWCNTs overlap with the Cr/Au electrodes by 1mm.

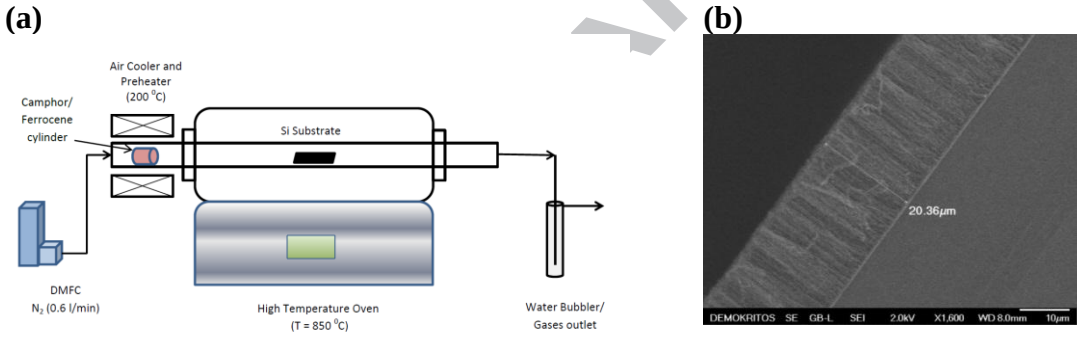

Fig. 1. (a) CVD Reactor for MWCNT growth (b) SEM picture of the MWCNTs produced

On some of the devices, a 100nm Indium Tin Oxide (ITO) over-layer was deposited using a RF magnetron sputtering Cooke 401 system. The microstructure of the sputtered ITO films was studied by XRD. The spectra indicated a fairly high polycrystalline phase. A total of 5 device variations were fabricated, each in 6 copies. They are shown in Fig. 2 and described in Table 1. They will be referred thereafter by their code names for simplicity.

ACCEPTED MANUSCRIPT

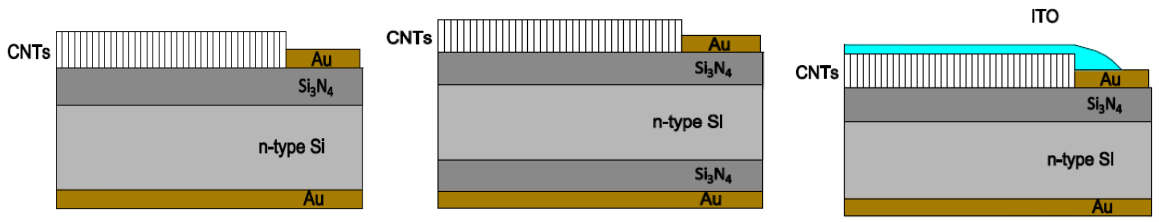

C **NC** **CI**

Fig.2. Device layout also described in Table 1.

Table 1

Device Variations

Name	*Description*
C	The basic device shown in Fig. 1b.
NC	Same as C, with an additional 140nm Si_3N_4 interlayer between the n-Si substrate and the bottom electrode.
CI	Same as C, with a 100nm ITO film overlapping the top Au electrode and the MWCNT film
CR	Reference structure to device C (subjected to the same high temperature process in the CVD reactor but without MWCNT deposition).
NCR	Reference structure to device NC (subjected to the same high temperature process in the CVD reactor but without MWCNT deposition).

2.3 XRF equipment

A micro-XRF study required for the identification of the presence of metals in the Si_3N_4 layer was carried out by means of a customized commercial portable micro-XRF spectrometer (Model Artax by Bruker-Nano) with optimized features regarding the design of the spectrometer head and the lens transmission efficiency at high energies (>20 keV). The spectrometer probe consisted of an X-Ray micro-focus Rh-anode tube (spot size 50 μm x 50 μm, max 50 kV, max 1 mA, 30W maximum power consumption, Be window of 0.2 mm thickness), a polycapillary X-ray lens as a focusing optical element with a focal distance equal to 21.2mm offering spatial resolution of about 50μm for Au-L_a characteristic X-rays. The X-ray detection chain consisted of an electro-thermally cooled 10 mm2 silicon drift detector (X-Flash, 1000B) with FWHM equal to 146 eV at 10kcps coupled with a digital signal processor. A color CCD camera (ca. 13 times magnification) is used for sample illumination and a dimmable white LED to produce a laser spot. Three different stepping motors, coupled with the spectrometer head, allow its three-dimensional movement, providing the possibility for linear/areal scanning measurements.

ACCEPTED MANUSCRIPT

2.4 Electrical and optical characterization equipment

A HP 4155A Semiconductor Parameter Analyzer and a HP 4140B pA/DC Voltage Source were used for static I-V measurements. A Signatone s-1041 Temperature Controller equipped with a hot chuck was used for temperature variation measurements. The light sources used for optical evaluation of the devices were (a) An Ushio UXL-150SO Xenon Arc Lamp combined with a Cornerstone 130 1/8 m Monochromator. (b) a Hamamatsu C-B3 S2-D2 UV source (c) a 275nm, 1mW LED (d) 405nm and 532nm, 10mW Lasers. The sources were calibrated with silicon photodetectors, a S120VC - Standard Photodiode Power Sensor by Thorlabs GmbH in the range 200-1100nm using a PM100USB - USB Power and Energy Meter Interface for C-Type Sensors by Thorlabs GmbH and a UV enhanced Newport 818-UV/DB sensor. The samples were mounted in a dark box allowing illumination through optical fibers. In all experiments the total optical power received by the sample did not exceed 200μW. An NDL-25C-4 (Thorlabs GmbH) Rectangular, Continuously Variable, Metallic Neutral Density Filter with Optical Density 0.04 - 4.0 was used for light intensity variation.

3.Results and Discussion

3.1 Metal diffusion into the upper Si_3N_4 layer

The MWCNT growth requires the use of a Fe catalyst. Additionally we opted to fabricate the Cr/Au electrodes before the MWCNT layer in order to protect them from damaging during the subsequent process steps. Therefore a diffusion barrier is required in order to prevent these metals from migrating into the silicon substrate, during the high temperature CVD step and this is the main purpose of the Si_3N_4 interlayer. The use of nitrides to act as metal diffusion barriers is a well-known property [13]. The interaction of Si_3N_4 with Fe has been particularly studied in the case of ceramic coatings for steel. Diffusion of Fe into the nitride is combined with the formation of Fe silicides[14] but in general Fe has not been used in mainstream Si fabrication processes.

In order to identify/correlate the presence of metallic impurities, scanning micro-XRF analysis was conducted on different samples. The line scan mode analysis was used with filtered excitation at 50kV, 600μA, 30s/measurement and with a scanning step of 0.1mm.

ACCEPTED MANUSCRIPT

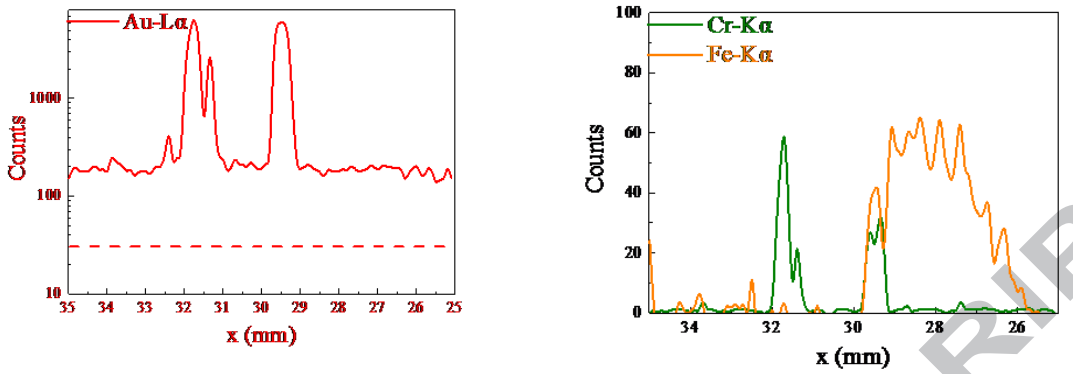

Fig. 3. Line scan across the electrode/MWCNT area of device CR. The electrodes extend in the regions 29-30mm and 31-32mm. The region 29-30 is the overlapping region between the electrode and the carbon layer which extends from 26 to 30mm (a) There is a significant background signal from Au demonstrating diffusion into the Si_3N_4 layer. (b) Cr and Fe also diffuse in small amounts outside the patterned areas.

When the CR device was examined, the Au-L_a lines were detected with higher intensity over the Cr/Au electrode as expected, however, elevated amounts were also found in the rest of the area under examination. The presence of Fe was confirmed as expected over the exposed area where the MWCNT would grow but small amounts were also detected elsewhere (Fig.3). This means that there is an extended contamination of the nitride layer due to Au and a limited damage due to Cr and Fe atoms. These metal atoms acting as traps contribute to a decrease of the resistivity of the Si_3N_4 layer.

3.2 Electrical Characterization

3.2.1 General overview

The I-V characteristics of the three basic structures present significant differences (Fig. 4a). C and NC devices behave as non-ideal Schottky diodes with a series resistance. The C device has the largest forward current while the inverse currents of C and NC are similar. The cutoff voltage derived by the tangent of the exponential part of the forward current shown in Fig. 4b are similar for C and CI (0.36V and 0.38V respectively) and a little higher in the NC case (0.45V). The CI device deviates from the thermionic emission model. A clear linear region in a log-log plot (Fig. 4c) is sustained up to 0.2V followed by a power law, an indication of the dominance of other mechanisms over thermionic emission. This will be discussed in subsection 3.2.3.

It was interesting to examine the detailed forward features of the I-V curves with respect to the reference devices not containing CNTs (Fig. 4d). The cutoff voltages of the CR and NCR references are 0.73 and 1.12V respectively, higher that of C and NC. The fact that they are drastically reduced when the CNT layer is added is a qualitative

ACCEPTED MANUSCRIPT

indication that the I-V characteristics of the reference devices depend mostly on the Schottky barrier height of Au/n-Si (0.79-0.80eV) while in the case of the C and NC devices the Schottky contact between the CNTs and n-Si dominates. Another feature evident in the reference devices is the presence of a low voltage space charge region (lower than 0.1V), which disappears when the CNTs are added. The series resistance is present in all devices, an indication that it is a substrate property[15].

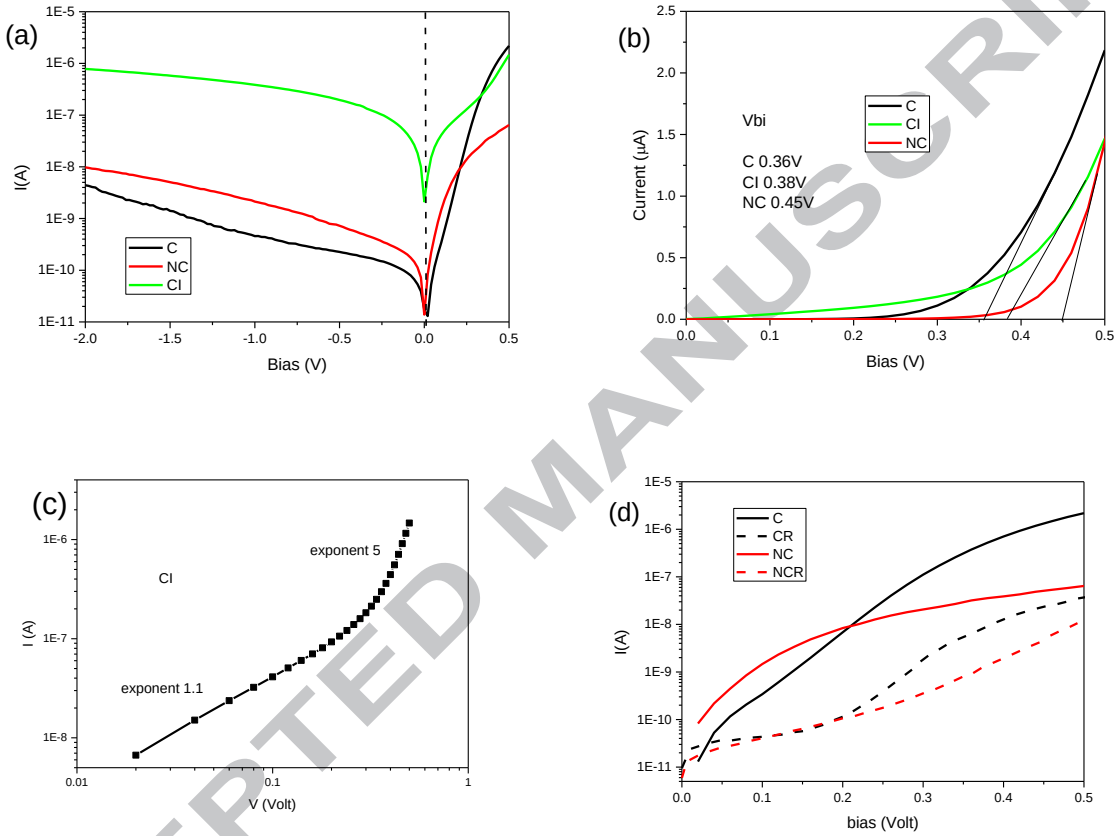

Fig. 4. Forward and inverse bias characteristics of the three devices C, NC and CI in room temperature conditions in logI plot (a) and at low forward bias (b). The Schottky contact dominates the transport behavior of C and NC while the CI device has a strong deviation from thermionic emission. In (c) a log-log plot of the forward characteristics of the CI is presented to demonstrate the deviation from thermionic emission. The IV of the C and NC structures are compared to references CR and NCR prepared under identical conditions but not containing the CNT layer (d)

3.2.2 Evaluation of Schottky diode parameters (C,NC)

The I-V relation in the case of a non-ideal Schottky diode with a series resistance is expressed by the following equations [15]:

$$I = I_s . e^{\frac{q(V-I.r_S)}{nkT}} (1 - e^{\frac{-q(V-I.r_S)}{kT}}) \quad (1)$$

ACCEPTED MANUSCRIPT

$$I_s = AA^*T^2 e^{\frac{-q\varphi_B}{kT}} \quad (2)$$

where A is the diode surface, A* the Richardson constant for the specific materials involved, n the ideality factor, included to take into account deviations from an ideal contact, φ_B the Schottky barrier height and r_s the series resistance. Relation (1) connects V to I in an implicit manner, however for lower current values, the terms involving the series resistance in the exponents can be simplified. A reliable method to evaluate I_s and n is based on the plot of the 'modified" logarithm of the current $mod(lnI) \equiv \ln\left(I/(1-\exp(-qV/kT)\right) = \ln(I_s) + \frac{qV}{nkT}$ (which comes from equation (1) for Ir_s << V) vs the bias voltage. In the case of low current values this reduces to a line and the intercept and slope provide I_s and n respectively (Fig. 5).

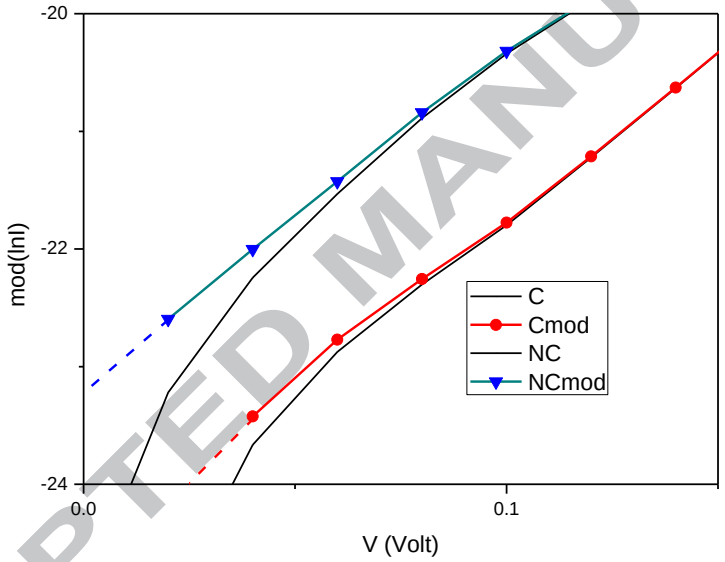

Fig. 5. Plot of the modified logarithmic current mod(lnI) vs. V at room temperature. The intercept provides I_s and n is derived from the slope q/nkT. The lnI values are also shown in the same plot.

Typical results at room temperature conditions are for device C: n=1.37 ± 0.02 and I_s=2.29 x 10^{-11}A and for NC n=1.34 ± 0.02, Is=8.8x10^{-11}A (Table 2). The ideality factor which is temperature dependent is significantly larger than unity and there is little differentiation between devices C and NC i.e. when the backgate nitride is added to the device. This means that the main generation recombination mechanisms in action that cause deviation from an ideal diode, such as Au or Fe traps in the nitride become important close to the upper interface where majority carriers are injected from the Si substrate in forward bias.

In order to evaluate the diode parameters, the temperature dependence of the I-V characteristics of all three types of devices were first measured. Results are shown in Fig.6 and Fig11a. Even before making any calculations it is evident from these plots that

ACCEPTED MANUSCRIPT

(a) the ideality factor must be temperature dependent and (b) the series resistance appearing for V>0.8V is almost temperature independent.

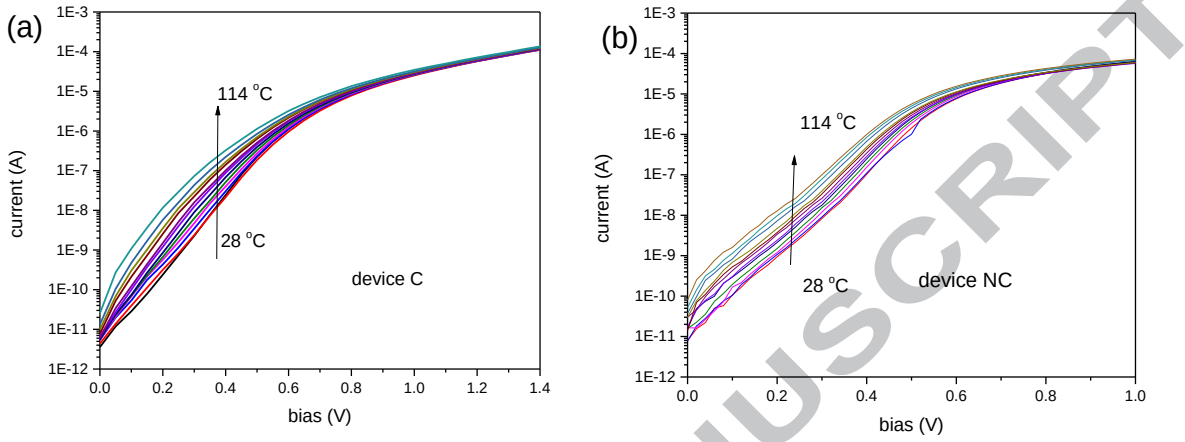

Fig. 6. Forward bias characteristics (a) of the C and (b) of the NC devices for a range of temperatures above ambient. These are used to evaluate both the quality factor and it's temperature dependence as well as the Schottky barrier height using the modified Norde function.

When temperature is increased the ideality factor decreases (Fig. 7) since thermionic emission is enhanced and for low voltages dominates carrier diffusion and generation-recombination mechanisms [16].

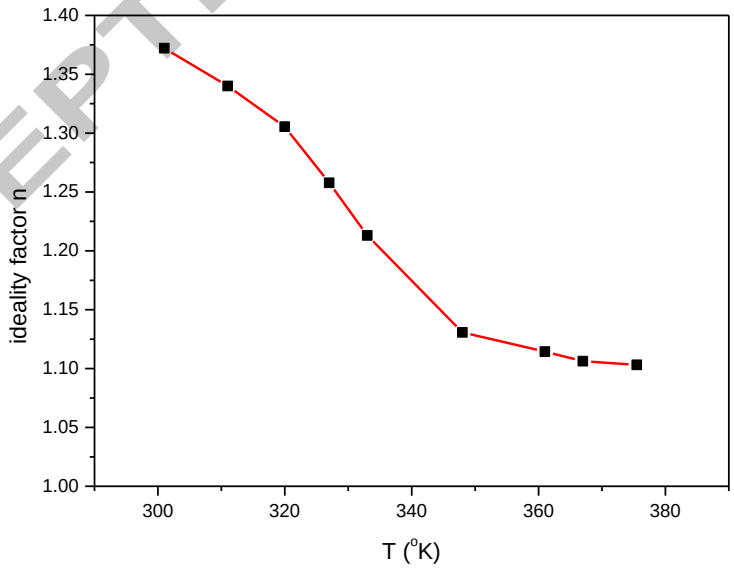

Fig 7. Dependence of the ideality factor upon temperature in the case of the C structure.

ACCEPTED MANUSCRIPT

The series resistance can be estimated directly from the I-V graphs, however a more accurate approach was selected. The experimental values I_i,V_i were used in combination with the theoretical expression (1) to formulate a least squares function with r_s as a parameter. The other parameters involved, namely n and I_s where obtained from the low voltage region. An example calculation at room temperature conditions is shown in Fig. 8. The values obtained for r_s are in the kOhm region in all temperature cases.

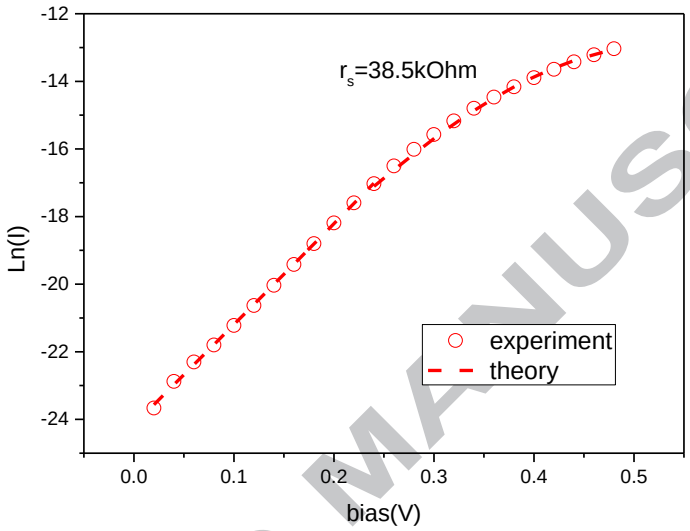

Fig.8. Example of evaluation of the series resistance by a least square fit approach involving the implicit theoretical expression (1) and experimental data for the C device at room temperature conditions.

The Schottky barrier height was evaluated by two different methods, the Richardson[17] extrapolation and the modified Norde method[15], [18]. The advantage of both methods is that they do not require the knowledge of the exact Richardson constant A^*. The Richardson method is derived from equations (1),(2). In the case of low forward bias the form $\ln\left(I/T^2\right) = \ln(AA^*) - (\varphi_B - \frac{V}{n})\, q/kT$ is derived which allows the evaluation of the barrier height for given low bias and ideality factor. The method works more consistently for devices C and NC. The case of the device CI is discussed in section 3.2.3. An example for device C is shown in Fig. 9.

ACCEPTED MANUSCRIPT

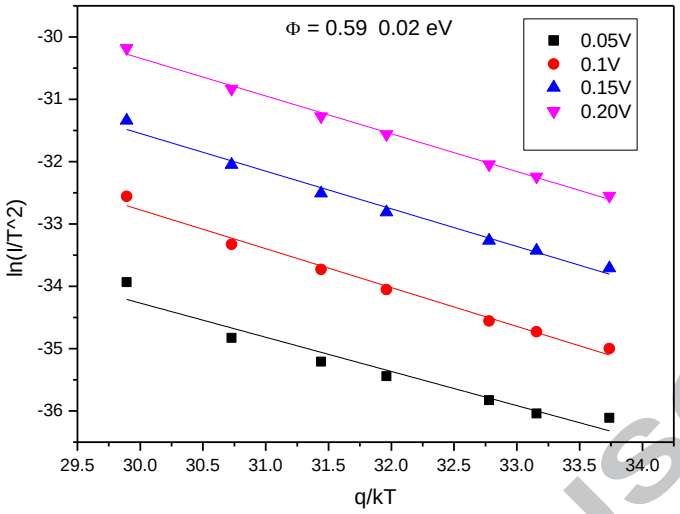

Fig 9. Example of a Richardson extrapolation on the data for the C device in forward bias.

The modified Norde method is a two-step approach demonstrated in Fig. 10 for the C device data of Fig.6. The first step is to plot function $F_1 = qV/2kT - \ln(I/T^2)$ vs. V for each temperature and locate the minima (Fig. 10a). These minima correspond to voltage and current values V_{min} and I_{min} which are used to formulate a second linear function $F_2 = 2F_{1min} + (2-n)\ln\left(\frac{I_{min}}{T^2}\right) = 2 - n[\ln(AA^*) + 1] + \frac{nq}{KT}\varphi_B$ with nq/kT as the independent variable. The slope provides the Schottky barrier shown in Fig. 10b.

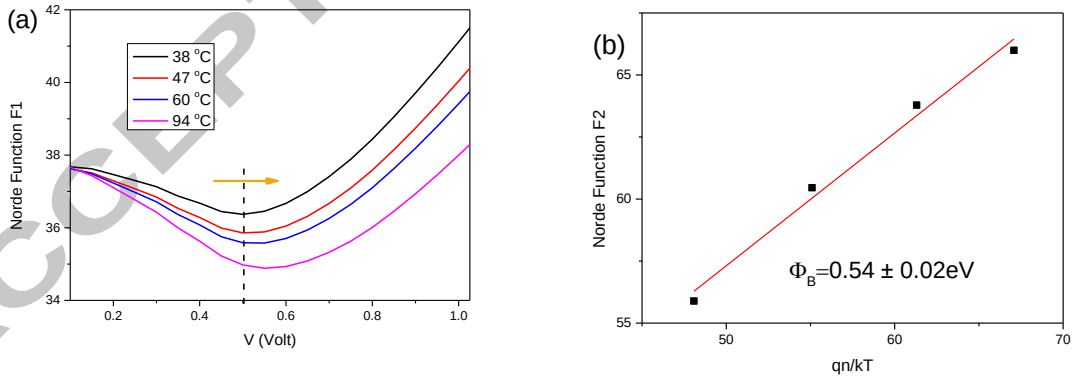

Fig. 10. Application of the Norde method for the evaluation of the Schottky barrier value for the C device (data of Fig 4a). (a) The minima of the function F_1 shift to the right (arrow) with temperature increase and they are used to formulate the second function F_2 (b).

A summary of the device parameters obtained is presented in Table 2.

ACCEPTED MANUSCRIPT

Table 2
Device parameters for C and NC

Device	V_{bi} (V)	I_s (A)	Ideality factor (temp.dep.)	Series Resistance (kΩ) (temp.dep.)	Φ_B Richardson (eV)	Φ_B Modified Norde (eV)
C	0.36	2.29×10^{-11}A	1.10-1.40	10-50	0.59	0.54
NC	0.45	8.8×10^{-11}A	1.25-1.54	10-50	0.45	0.38

3.2.3 Transport mechanisms in device CI

The inclusion of the ITO overlayer significantly modifies the transport mechanisms in the geometry used. The overall experimental result for I-V is shown in Fig. 4c. The linear part at low voltage bias persists up to 0.2V (not consistent with the thermionic emission law equation (1)) while for higher voltages a power exponent 5.0 suggests transport in the presence of traps[19]. A Richardson plot $\ln(I/T^2)$ vs q/kT similar to Fig. 9 for low voltage bias is still possible and the resulting barrier height is 0.12 eV. The difference between the work function of ITO (4.26-4.42 eV when it is deposited by sputtering) [20], [21] and that of silicon (4.05eV) is between the limits 0.21-0.37eV and this suggests that part of the ITO layer which is in direct contact with the nitride contributes in lowering significantly the metal Schottky barrier. In this case transport is monitored mainly by the traps inside the nitride. Transport in nitride films has been studied for a large range of thicknesses and resistivities[22]. The suggested mechanisms include Poole-Frenkel, Fowler-Nordheim tunneling and hopping conductance through traps in the insulator. This latter mechanism described by $I \sim V.\exp(-E_a/kT)$ is temperature dependent and fits best our experimental data in the linear region <0.2V (Fig. 11b). The activation energy evaluated is Ea=0.157±0.004eV. The overall result of lowering the Schottky barrier for a light detector application is an undesirable increase of the dark current.

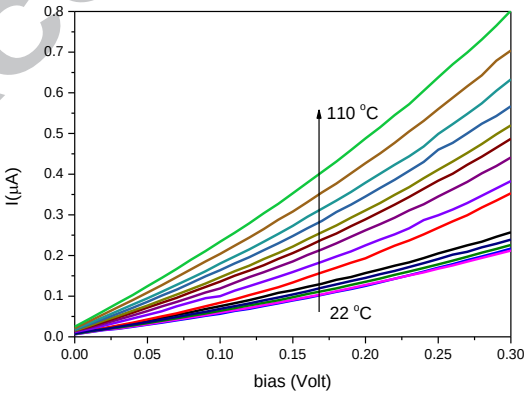

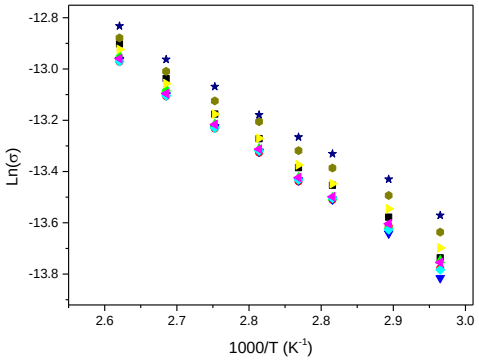

ACCEPTED MANUSCRIPT

Fig. 11. (a) I-V characteristics of the CI device in the temperature range 22-110 ^{o}C and voltages up to 0.3V. (b) Hopping conductance vs inverse temperature for low biases. The resultant activation energy is Ea=0.157±0.004 eV

3.3 Optical Characterization

3.3.1 Visible spectrum

The optical response and performance of the devices was tested first in the visible spectrum either for specific wavelengths or at a broader spectrum in the range 200nm-1000nm. An important issue in this study is the influence of the back nitride and front ITO layers (devices NC, CI) on the performance of the basic device C and the correlation to the I-V characteristics of the devices.

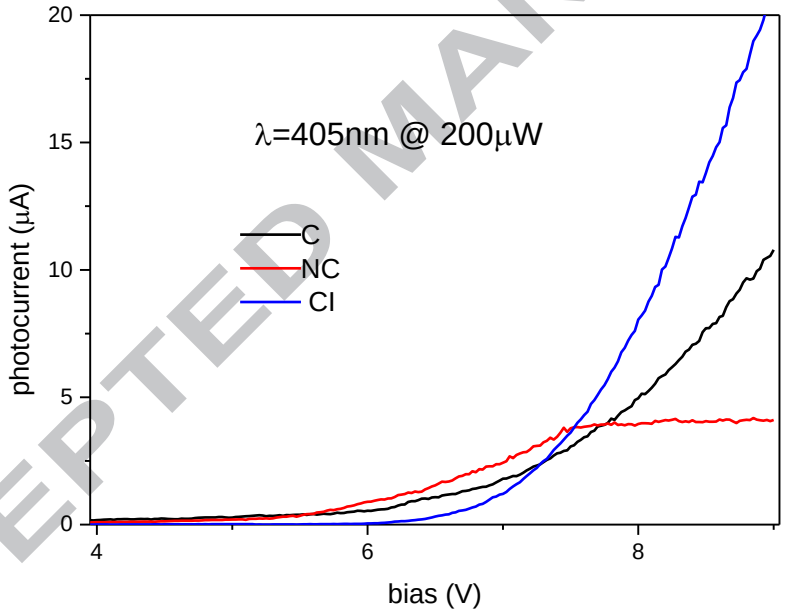

Fig.12. Photocurrent vs bias voltage in the case of a monochromatic source. The device surface is 0.30cm^2.

In Fig. 12 the photocurrent vs bias is shown in the case of a 405nm LASER source through an optical fiber. In all cases the device response starts at about 5.5V, a threshold related the Schottky n-type Si/Au device and not influenced by the presence of the other layers. Saturation of the photocurrent occurs for biases >9V. The presence of the backgate nitride causes earlier saturation since tunneling effects dominate other current transport mechanisms. The addition of the ITO layer (device CI) results in better photo

ACCEPTED MANUSCRIPT

carrier collection compared to the non-capped devices (C and NC) due to increase of the homogeneity of the electric field on the surface [23], [24]. On the other hand, due to the limited transparency of ITO in the UV and IR region , its use is only beneficial in the visible part of the spectrum.

When examined in the region 200-1000nm at relatively low light power (1-2 μW) the C devices prove to be comparable to a standard commercial UV enhanced photodiode (Fig. 13a) in terms of responsivity. The presence of the ITO layer (device CI) results in less noisy response however the device is less sensitive. The addition of a nitride back-layer (device NC) further decreases the photocurrent.

In terms of Equivalent Quantum Efficiency (EQE)[1] the C device is also comparable to the reference with a peak of 80% around 750nm and a minimum of 40% at 210nm (Fig. 13b) at a bias of 9V.

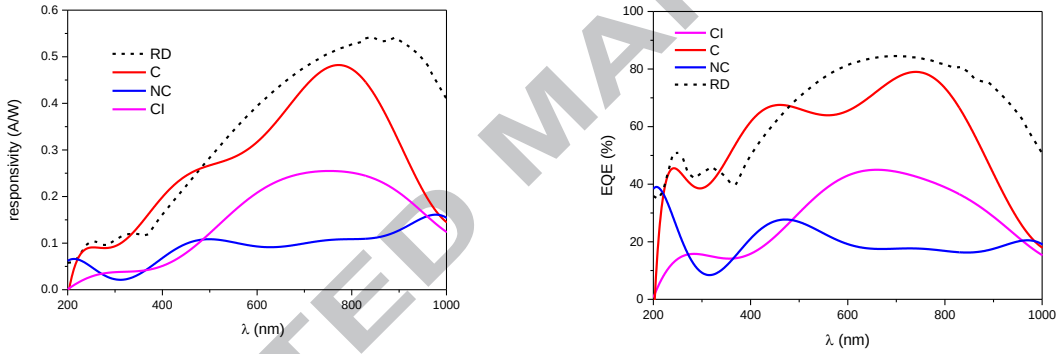

Fig 13. Optical responsivity (a) and EQE (b) of the devices in the 200-1000nm optical part of the spectrum. The data for a commercial UV- enhanced silicon photodetector (Newport 818-UV) have been also included for reference (dotted line RD). The bias voltage used 9V.

3.3.2 UV spectrum (275 nm LED source)

The optical features of the basic structure (device C) where tested with a monochromatic source at 275nm. An optical power range of 1-200μW was examined. Fig. 14a shows the responsivity and EQE for a fixed power vs the bias voltage. A peak of 120mA/W and 55% EQE was observed for 7.5V bias and 1μW power. For higher voltage biases the response decreases. This saturation effect is also power dependent. Beyond a specific power value which is bias dependent the photocurrent does not increase further with the increase of the incident power (Fig 14b). In the case examined a peak value for the responsivity of about 220mA/W and the EQE 90% was obtained for a

ACCEPTED MANUSCRIPT

power of 0.3μW and bias 7V. These values settle to 90mA/W and EQE of 35% for power values > 0.8W in compliance with Fig.13.

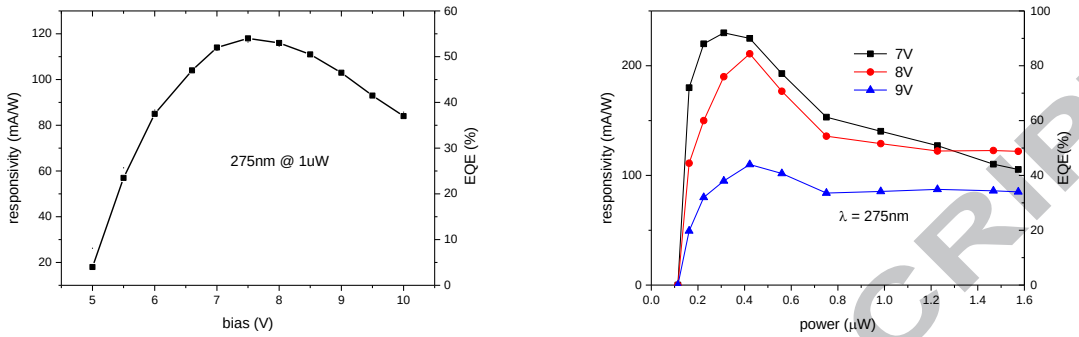

Fig. 14. Response of the basic device to a 275nm monochromatic source vs the bias voltage (a) and vs the incident power (b)

4. Conclusions

We fabricated metal-semiconductor photodetectors based on standing carbon nanotubes. A low conductance silicon nitride layer containing Au and Fe traps deposited during the process was used to reduce the inverse bias dark current and act as a diffusion barrier to protect the Si substrate. The basic device (C) was compared against devices containing an additional backside silicon nitride (NC), a device with an ITO cover of the CNT tubes (CI) and reference devices (CR, NCR) not containing the CNTs. The role of each component was evaluated by electrical and optical characterization. The addition of the backside silicon nitride (NC) resulted indeed in the reduction of the dark current but with the serious side-effect of increasing the influence of generation-recombination. The ITO overlayer (CI) had the beneficial effect of reducing noise and providing better contact with the CNTs however a serious reduction of the Schottky barrier was observed resulting in an almost ohmic behavior under inverse bias. Nevertheless the performance of the CI photodetector in the visible part of the spectrum was comparable to commercial standards. Overall the results suggest that the basic structure C had the best performance as a UV detector (EQE 90% @ 275nm@ 7V). This work demonstrates that CNT based devices have a potential for UV applications.

Acknowledgements : We would like to thank Dr. George Stavropoulos from the Institute of Nuclear and Particle Physics of NCSR "DEMOKRITOS" for his kind offer of a set of optical devices used for the optical characterization of our system and Dr. Andreas Karydas from the Institute of Nuclear and Particle Physics of NCSR "DEMOKRITOS" for sharing his experience about XRF studies and the fruitful discussions about the XRF results.

ACCEPTED MANUSCRIPT

This research did not receive any specific grant from funding agencies in the public, commercial, or not-for-profit sectors.

REFERENCES

[1] X. He, F. Leonard, and J. Kono, "Uncooled Carbon Nanotube Photodetectors," *Adv. Opt. Mater.*, vol. 3, no. 8, pp. 989–1011, 2015.

[2] M. Richter, T. Heumuller, G. J. Matt, W. Heiss, and C. J. Brabec, "Carbon Photodetectors: The Versatility of Carbon Allotropes," *Adv. Energy Mater.*, vol. 7, no. 10, 2017.

[3] A. Behnam *et al.*, "Metal-semiconductor-metal photodetectors based on single-walled carbon nanotube film – GaAs Schottky contacts," *J. Appl. Phys.*, pp. 1–6, 2008.

[4] F. Rao, X. Liu, T. Li, Y. Zhou, and Y. Wang, "The synthesis and fabrication of horizontally aligned single-walled carbon nanotubes suspended across wide trenches for infrared detecting application," *Nanotechnology*, vol. 20, no. 5, 2009.

[5] R. Lu, Z. Li, G. Xu, and J. Z. Wu, "Suspending single-wall carbon nanotube thin film infrared bolometers on microchannels," *Appl. Phys. Lett.*, vol. 94, no. 16, pp. 92–95, 2009.

[6] P. Ong, W. B. Euler, and I. A. Levitsky, "Carbon nanotube-Si diode as a detector of mid-infrared illumination," *Appl. Phys. Lett.*, pp. 3–5, 2010.

[7] L. Xiao *et al.*, "A polarized infrared thermal detector made from super-aligned multiwalled carbon nanotube films," *Nanotechnology*, vol. 22, no. 2, 2011.

[8] R. Lu, C. Christianson, B. Weintrub, and J. Z. Wu, "High photoresponse in hybrid graphene-carbon nanotube infrared detectors," *ACS Appl. Mater. Interfaces*, vol. 5, pp. 11703–11707, 2013.

[9] Y. An, H. Rao, G. Bosman, and A. Ural, "Characterization of carbon nanotube film-silicon Schottky barrier photodetectors," *J. Vac. Sci. Technol. B, Nanotechnol. Microelectron. Mater. Process. Meas. Phenom.*, vol. 30, no. 2, p. 21805, 2012.

[10] D. Melisi *et al.*, "Radiation detectors based on Multiwall Carbon Nanotubes deposited by a spray technique," *Thin Solid Films*, vol. 543, pp. 19–22, 2013.

[11] D. Melisi *et al.*, "Photodetectors based on carbon nanotubes deposited by using a spray technique on semi-insulating gallium arsenide," *Beilstein J.Nanotechnol.*, vol. 5, pp. 1999–2006, 2014.

[12] C. Aramo *et al.*, "Progress in the realization of a silicon-CNT photodetector," *Nucl. Inst. Methods Phys. Res. A*, vol. 695, pp. 150–153, 2012.

ACCEPTED MANUSCRIPT

[13] S. Q. Wang, I. Raaijmakers, B. J. Burrow, S. Suthar, S. Redkar, and K. B. Kim, "Reactively sputtered TiN as a diffusion barrier between Cu and Si," *J. Appl. Phys.*, 1990.

[14] R. Polanco, A. De Pablos, P. Miranzo, and M. I. Osendi, "Metal-ceramic interfaces: Joining silicon nitride-stainless steel," *Appl. Surf. Sci.*, vol. 238, no. 1–4 SPEC. ISS., pp. 506–512, 2004.

[15] D. K. Schroder, *SEMICONDUCTOR MATERIAL AND DEVICE CHARACTERIZATION, Third Edition*, vol. 44, no. 4. 2006.

[16] R. Sharma, "Temperature Dependence of I-V Characteristics of Au/n-Si Schottky Barrier Diode," *J. Electron Devices*, vol. 8, no. September, pp. 286–292, 2012.

[17] R. T. Tung, "The physics and chemistry of the Schottky barrier height," *Appl. Phys. Rev.*, vol. 1, p. 011304 1-50, 2014.

[18] T. Chot, "A Modified Forward I-V Plot for Schottky Diodes with High Series Resistance," *phys. stat. sol.*, vol. 66, pp. 43–45, 1981.

[19] Z. A. K. Durrani and M. A. Rafiq, "Electronic transport in silicon nanocrystals and nanochains," *Microelectron. Eng.*, vol. 86, no. 4–6, pp. 456–466, 2009.

[20] Y. Park, V. Choong, Y. Gao, B. R. Hsieh, and C. W. Tang, "Work function of indium tin oxide transparent conductor measured by photoelectron spectroscopy," *Appl. Phys. Lett.*, vol. 68, no. 19, pp. 2699–2701, 1996.

[21] R. Schlaf, H. Murata, and Z. . Kafafi, "Work function measurements on indium tin oxide films," *J. Electron Spectros. Relat. Phenomena*, vol. 120, no. 1–3, pp. 149–154, 2001.

[22] S. M. Sze, "Current transport and maximum dielectric strength of silicon nitride films," *J. Appl. Phys.*, vol. 38, no. 7, pp. 2951–2956, 1967.

[23] A. Valentini *et al.*, "A conductive surface coating for Si-CNT radiation detectors," *Nucl. Instruments Methods Phys. Res. Sect. A Accel. Spectrometers, Detect. Assoc. Equip.*, vol. 790, pp. 14–18, 2015.

[24] D. Alonso-Álvarez, L. Ferre Llin, N. J. Ekins-Daukes, and D. J. Paul, "ITO and AZO films for low emissivity coatings in hybrid photovoltaic-thermal applications," *Sol. Energy*, vol. 155, pp. 82–92, 2017.

ACCEPTED MANUSCRIPT

ACCEPTED MANUSCRIPT

Anastasia-Sofia Filatzikioti received her Diploma in *Applied Physics* from the National Technical University of Athens, Greece, 2014 and her MSc in *Microsystems and Nanodevices* from the same university, 2017. She conducted her postgraduate thesis within Professor's N.Glezos team at the Institute of Nanoscience and Nanotechnology at NCSR "Demokritos" in Athens. Her research interests include a wide range of topics, from Micro- and Nano-systems' fabrication processes and Organic Nanomaterials to Physics of Semiconductors and Microfluidic Mechanics.

Dr Nikos Glezos received his B.Sc. in Physics from the University of Athens, 1979 and his Ph.D. in Solid State Physics from the same university, 1984. He is a Director of Research in the Institute of Nanoscience and Nanotechnology (INN) of NCSR "Demokritos" in Athens, Greece. His research interests are electron beam lithography process and process simulation, molecular electronic devices and charge transport in the nanoscale. He is currently working on molecular memories and optical sensors.

Dr. Vasiliki Kantarelou received her B .Sc in Physics from the University of Patras, 1995 and her Ph.D. on X-Ray Fluorescence spectroscopy from the National Technical University of Athens, 2006. She is a Research Associate in the Institute of Nuclear and Particle Physics (INPP) of NCSR "Demokritos" in Athens, Greece. Her research interests

ACCEPTED MANUSCRIPT

are the development, evaluation and application of a micro-X ray fluorescence spectrometer on cultural heritage. She is currently working in laboratory of material analysis in INPP.

Dr Aristotelis Kyriakis received his B .Sc in Physics from the University of Patras, 1989 and his Ph.D. in Particle Physics from the National Technical University of Athens, 1994. He is a Senior Researcher in the Institute of Nuclear and Particle Physics (INPP) of NCSR "Demokritos" in Athens, Greece. His research interests are solid state sensor development and electronics design and physics analysis in the framework of LHC experiments. He is currently working on the Silicon strip tracker upgrade of the CMS/LHC experiment.

Dr. George Pilatos graduated from the School of Chemical Engineering at the National Technical University of Athens in 1997. He also received a doctorate NTUA thesis in synthesis of graphitic nanostructures. He is a permanent Research scientist in the Institute of Nanoscience and Nanotechnology (INN) of NCSR "Demokritos" in Athens, Greece. His research interests are synthesis and characterization of activated carbon and graphitic nanostructures, CNTs and Graphenes.

ACCEPTED MANUSCRIPT

ACCEPTED MANUSCRIPT

Dr George Romanos received his B.Sc in Chemical Engineering from the National Technical University of Athens (NTUA), 1994 and his Ph.D. in Physical Chemistry from the same university, 2001. He is a Director of Research at the Institute of Nanoscience and Nanotechnology (INN) of NCSR "Demokritos" in Athens, Greece. His research interests are on Nanoporous Materials and Membranes Development, Characterisation and Applications. He is currently working on Carbon Nanotube and Graphene Membranes and adsorbents for gas separation and water treatment.

Dr Thanassis Speliotis, received his B .Sc in Physics from the Aristotle University of Thessaloniki (AUTh), 1989 and his Ph.D. in Experimental Solid State Physics from the National Technical University of Athens (NTUA), 1999. He is Senior Researcher in the Institute of Nanoscience and Nanotechnology (INN) of NCSR "Demokritos" in Athens, Greece. His research interests are Magnetic Materials, Thin Films, 2D materials, Nanotechnology and Device Physics and Galvanomagnetic Phenomena

Demetra Stathopoulou received her B. Sc in Physics from the University of Athens in 2004 and her M. Sc in the field of Microsystems and Nanodevices from the School of Applied Mathematics and Physical Sciences at the National Technical University of

ACCEPTED MANUSCRIPT

Athens in 2017. She is currently a Phd candidate at the University of Peloponnese working on her thesis in the field of Optical Communication Systems.

ACCEPTED MANUSCRIPT

ACCEPTED MANUSCRIPT

Highlights

- We fabricate a hybrid MWCNT/Si_3N_4/n-Si photodetector based on ordered MWCNTs and evaluate its performance in the UV, visual and near IR spectrum (200-1000nm).
- The basic device and some meaningful variations including additional layers are electrically and optically tested and compared.
- The overall results suggest that all devices had a satisfactory performance in the visual part of the spectrum and that the basic structure had the better performance as a UV detector (EQE 90% @ 275nm@ 7V).
- The aim of this work is to demonstrate that the growth of dense ordered MWCNTs can be successfully combined with other semiconductor clean room processes in order to fabricate photodetectors, provided that the side effects are taken into account and the process flow is selected appropriately.

ACCEPTED MANUSCRIPT